



HAL
open science

Atmospheric boundary layer modeling in a short wind tunnel

Dan Hlevca, Mircea Degeratu

► **To cite this version:**

Dan Hlevca, Mircea Degeratu. Atmospheric boundary layer modeling in a short wind tunnel. European Journal of Mechanics - B/Fluids, 2020, 79, pp.367 - 375. 10.1016/j.euromechflu.2019.10.003 . hal-03488921

HAL Id: hal-03488921

<https://hal.science/hal-03488921>

Submitted on 20 Jul 2022

HAL is a multi-disciplinary open access archive for the deposit and dissemination of scientific research documents, whether they are published or not. The documents may come from teaching and research institutions in France or abroad, or from public or private research centers.

L'archive ouverte pluridisciplinaire **HAL**, est destinée au dépôt et à la diffusion de documents scientifiques de niveau recherche, publiés ou non, émanant des établissements d'enseignement et de recherche français ou étrangers, des laboratoires publics ou privés.



Distributed under a Creative Commons Attribution - NonCommercial 4.0 International License

Atmospheric boundary layer modeling in a short wind tunnel

Dan Hlevca · Mircea Degeratu

Received: date / Accepted: date

Abstract The aim of the study was to analyze and design through experimental and numerical investigations a passive device to control the development of the boundary layer in an existing short wind tunnel to reproduce conditions representative of an atmospheric boundary layer for wind engineering applications. The current main use of the tunnel being for automotive and train aerodynamics, constrained the design to look for a reversible solution. The approach followed was then to install a grid of horizontal bars of squared cross-section with different dimensions at the entrance of the experimental chamber. The distribution of the bars was selected to be symmetric with respect to the horizontal longitudinal mid-plane of the tunnel. The approach has been validated through experimental measurements by hot-wire anemometry and numerical simulations based on finite volume RANS of the full wind tunnel geometry. The analysis showed that the grid acting as a passive flow control device was effective to reproduce in a short wind tunnel the main characteristics of an atmospheric boundary layer.

Keywords

wind tunnel atmospheric boundary layer development, passive flow control, atmospheric turbulence, wind engineering.

1 Introduction

The urban landscape of modern cities around the world was changed by slender buildings. Their design requires determining wind induced loads issued from models whose validity needs to be established through wind tunnel testing. Furthermore, associated with the diffusion and dispersion of pollutants in the atmosphere, appropriate flow conditions need to be reproduced in experimental wind tunnel testing. In order to properly account for these phenomena and principles and reproduce “real“ wind conditions, one needs to ensure that the atmospheric boundary layer (ABL) conditions are reproduced in wind tunnel. Usually, wind tunnel facilities used for applications other than wind engineering must satisfy constraints such as flow uniformity and low turbulence fluctuations. Consequently, as such, they cannot be used as a tool to investigate problems occurring inside the atmospheric boundary layer (ABL) where, generally, the flow is characterized by a rather irregular velocity profile and a high level of turbulence. These properties are critical for predicting wind loads on large structures and they are rather difficult to simulate in wind tunnel [27]. This paper deals with an experimental and numerical study carried out to identify the proper design parameters allowing the development

D. Hlevca
DynFluid Laboratory, Arts et Métiers ParisTech, France
E-mail: dan.hlevca@gmail.com

M. Degeratu
Technical University of Civil Engineering Bucharest, Hydraulics and Environmental Protection Department,
Bucharest, Romania
E-mail: mircea.degeratu@yahoo.com

of ABL in a short wind tunnel. The ultimate goal of the work being to convert an existing wind tunnel originally designed for automotive and train aerodynamics applications into a facility where the atmospheric boundary layer is correctly reproduced. Methodologies for designing wind tunnels used for specific purposes: wind loads on buildings, dispersion of air pollution, pedestrian comfort, drifting and deposition of ice and snow, influence of wind and heating on structures were developed by the authors of [3], [4] and [1]. A wind tunnel with two experimental chambers was designed by Diana [11] and can be used for both aeronautical and wind engineering applications. In our case, one of the challenges is to make the conversion of the tunnel reversible in order to be able to use the facility for both applications whenever needed. According to [16], the methods used to obtain the development of the ABL in a short wind tunnel usually consist of using roughness elements in combination with barriers and mixing devices. These methods are called RBMD (Roughness Barrier and Mixing Devices) [10], and have been used for the first time by [6]. The latter showed that in the absence of thermal effects the turbulence dynamics is driven by terrain roughness [8]. RBMD methods were and still are considered the best techniques in representing the dynamics characteristics of ABL in short wind tunnels. However, they have the disadvantage that the length of the test chamber must be significantly long to attain ABL conditions.

In the present work the analysis is focused on the use of a passive flow control device to reproduce the ABL in a short wind tunnel (i.e. having a short experimental test chamber). The device was designed through both numerical simulations and experiments, and consists of horizontal bars of squared cross-section being evenly spaced and having different dimensions arranged in a grid and installed at the entrance of the test chamber. The existing wind tunnel has a 3m x 5m test chamber with slotted walls for passive boundary layer control and 10 m in length. Because of the scale of the facility, the analysis and validation of the modification of the wind tunnel are expensive in terms of resources. In order to reduce the costs, the analysis was then carried out in a reduced scale facility with a three quarter open test chamber (1:5 scale factor of with respect to the original facility). In order to make the test chambers of the two wind tunnels geometrically similar, the smaller wind tunnel has been modified by introducing a cage with slotted walls in the test chamber reproducing the original large scale one. The overall flow characteristics were first assessed by performing three-dimensional numerical simulations of the flow in the empty wind tunnel (i.e. without the passive flow control device addressed as FP hereafter). In order to determine the “optimal” dimensions and spacing of the horizontal bars, two-dimensional numerical simulations were first performed considering the longitudinal vertical mid plane of the FP test chamber. The resulting bars were then manufactured and assembled into a grid that was installed at the upstream end of the experimental chamber downstream of the honeycomb (hereafter we refer to the modified reduced scale facility as modified FP). Experiments and numerical simulations of the full modified wind tunnel geometry were then carried out, and the influence of the bars was evaluated by means of numerical simulations and experiments. The velocity profiles, turbulent intensity, turbulent length scales and power spectra of the longitudinal component of velocity were also compared with semi-analytical laws given in the literature. The atmospheric boundary layer characteristics, the experimental setup and numerical approach are presented in the following sections. Then the results are discussed and concluding remarks are given.

2 Atmospheric boundary layer characteristics

A neutral atmospheric boundary layer (i.e. absence of thermal stratification) is considered in the present study. For wind engineering applications, reproducing such an ABL is a key issue both for experimental and numerical simulations and one has to accurately reproduce the main characteristics of the ABL, namely: the mean velocity profile, the turbulence intensity level, the integral length scale and the power spectral density ([6], [9], [17]). In the lower part of an atmospheric boundary layer (20-30% above the surface), the mean velocity exhibits a logarithmic behavior

$$u(z) = \frac{1}{K} u_\tau \ln\left(\frac{z}{z_0}\right) \quad (1)$$

where z_0 is the roughness length that depends on the type of the terrain, u_τ is the friction velocity ($u_\tau \simeq 1 - 2$ m/s for extreme winds) and K is the Von Karman constant ($K=0.41$)[26]. For open sea, ice, tundra or desert $z_0 = 0.001$; for open country with low scrub or scattered trees $z_0 = 0.03$; for suburban area, small towns and well wooded areas $z_0 = 0.3$; and for tall buildings and city centers $z_0 = 3$, where z and z_0 values are expressed in dimensional units (meters).

In the majority of wind engineering applications, the distribution of the mean velocity profile of the atmospheric boundary layer is generally well represented by the power law approximation

$$\frac{U_1}{U_2} = \left(\frac{z_1 - d}{z_2 - d} \right)^\alpha \quad (2)$$

where subscripts 1 and 2 refer to two different heights in the boundary layer, and $\alpha = 0.14 - 0.17$ for rural terrain, $0.21 - 0.27$ for suburban terrain and $0.28 - 0.35$ for urban terrain ([9], [17]).

The turbulent intensity is computed with respect to the local mean velocity (\bar{u}):

$$I_u = \frac{\sigma_u}{\bar{u}} \quad (3)$$

where σ_u is the standard deviation of the longitudinal velocity signal, and the turbulent integral length scale is calculated from the autocorrelation function according to

$$L_u = \bar{u} \int R_{uu}(r) dr \quad (4)$$

where R_{uu} is the autocorrelation of the longitudinal fluctuations.

The power spectral densities of the ABL are generally found to obey the Von Karman spectrum expressions

$$\frac{f S_u(f)}{\sigma_u^2} = \frac{4f_u}{(1 + 70.8f_u^2)^{5/6}} \quad (5)$$

$$\frac{f S_v(f)}{\sigma_v^2} = \frac{4f_v(1 + 755.2f_v^2)}{(1 + 283.2f_v^2)^{11/6}} \quad (6)$$

where $f_i = fL_i/U$, f is the frequency and U is the average longitudinal wind velocity that was obtained by time averaging the hot wire measurements at given locations in the mid-longitudinal plane of the test section.

3 Experimental setup and numerical approach

The aim of the study was to design, by means of experimental and numerical investigations, a passive device to control the development of the boundary layer in a short wind tunnel originally used for automotive and train aerodynamics (the S4 wind tunnel of Institut Aérotechnique, referred to as S4), so as to reproduce conditions representatives of an atmospheric boundary layer for wind engineering applications.

The S4 has a closed circuit with a test section of 3 m (height) by 5 m (width), a useful length of 7 m, and slotted walls to reduce blockage effect. The maximum attainable speed in the test chamber is 40 m/s with a unit Reynolds number $Re = 4.17 \cdot 10^6$ (calculated with the height of the ABL which is 1.5 m). The distance between the entrance of the test chamber and the first reliable measurement location is only 3 m and it is not sufficient for the boundary layer to develop, reaching conditions representatives of an ABL. In order to reproduce such conditions a device consisting of a grid of horizontal bars of different squared cross sections installed at the entrance of the test chamber was analyzed. In order to fabricate and to test the grid several steps were carried out: (i) preliminary 2-D simulations were performed to optimize spacing and cross section size (d) of the bars ; (ii) the device was fabricated, installed and tested in a reduced scale wind tunnel (FP) modified to replicate the geometry of S4; and (iii) numerical simulations of the full reduced scale wind tunnel geometry were carried out to analyze the influence of the geometrical parameters.

The use of FP allowed us to minimize resources for the design and manufacturing of the device. For that purpose, slotted walls in plexiglas with the same geometrical characteristics of the S4 walls but at a scale 1:5 were fabricated and installed in the test chamber of the FP (see figure 6). The function of the slotted walls is to create the reduced scale wind tunnel (FP) geometrically similar to the large scale wind tunnel (S4). Air flows through a nozzle having a contraction ratio of 15 and it passes through a honeycomb before entering the test chamber. The velocity can be varied between 0 and 25 m/s and the maximum turbulence level is less than 1%. The unit Reynolds number is $Re = 0.504 \cdot 10^6$ (calculated with the height of the ABL which is 0.3 m). A schematic representation of the wind tunnel is given in figure 1.

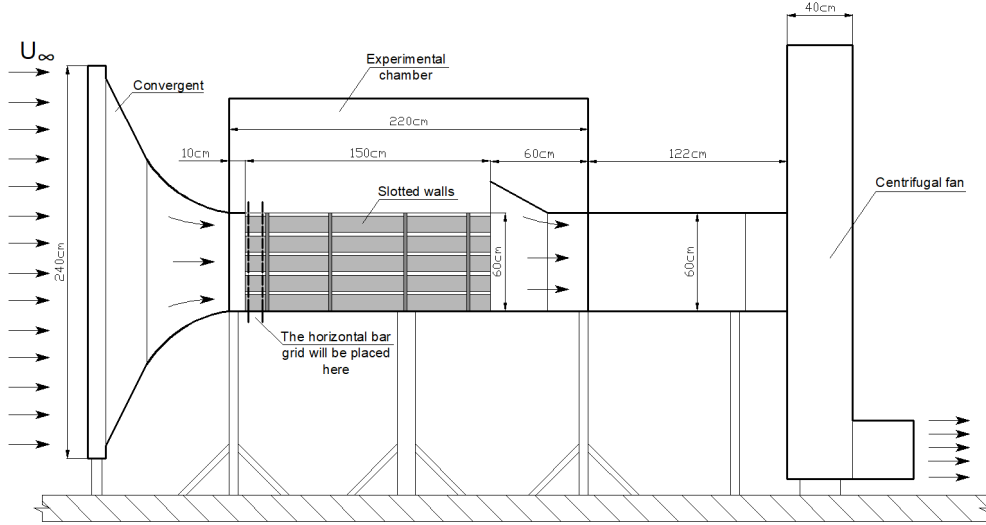


Fig. 1: Schematic representation of the reduced scale wind tunnel.

Unsteady velocity measurements have been performed using a Dantec StreamLine hot-wire anemometer running in constant-temperature for three different wind velocities. Measurements were taken at three different streamwise locations in the lower half of the mid-longitudinal vertical plane ($x - z$ plane) of the experimental test chamber. Two measurements campaigns have been carried out. In the first one the velocity has been measured and the turbulence intensity computed from the data extracted every 2 mm in the (z) transverse direction for a total of 150 points/measurement with a 1D hot wire probe (type 55P15). In the second campaign measurements were taken with a 2D hot wire probe (type 55P61) at 29 different transverse positions spanning from 2mm to 302mm (11 points from 2mm to 7mm; 5 points from 8 to 12mm; 4 points from 17 to 32mm; and 9 points from 62 to 302mm) and the integral length scale and the power spectral density were calculated. The uncertainties of the hot wire measurements were found to range up to 0.45% error. This value represents the curve fit errors associated with the calibration of the hot wire, and it defines the deviation between the measured velocity and the velocity calculated by curve fitting. This value is expressed as a percentage of the measured value.

The numerical simulations of the flow have been carried out considering both the full three-dimensional and the two-dimensional geometry (thus corresponding to the longitudinal vertical mid plane). The analysis was based on the incompressible Reynolds Averaged Navier-Stokes equations where the SST $k - \omega$ turbulence model of Menter [21] was used for closure. A commercial code (ANSYS Fluent) was used to solve RANS equations. The solver relies on a segregated finite volume formulation based on a coupled solution algorithm for pressure-velocity and second order upwind spatial discretization scheme. The geometry was modeled and discretized by means of Gambit v2.4.6 (for more details refer to [2]).

4 Results and discussion

The present work deals with the modeling of an atmospheric boundary layer in a short wind tunnel by means of a passive flow control device composed of a grid of bars of squared cross-sections placed horizontally in the transverse direction. In order to design such a device and characterize its effects, both experimental investigations and numerical simulations were carried out. To calibrate the model parameters, the selected turbulence model and grid resolutions, preliminary three-dimensional simulations of the flow inside the empty FP wind tunnel (i.e. no bars were present) were performed.

In order to optimize the arrangement of the bars, namely determining their size and cross-section dimensions and spacing in the vertical direction, two-dimensional simulations considering the mid longitudinal plane ($x - y$ plane) of the FP were first performed. Having the optimized geometrical parameters, 3D simulations of the full reduced scale wind tunnel FP were performed.

An experimental investigation has been carried out, on one hand to validate the numerical simulations, on the other to characterize the properties of the flow. The investigations relied on the use of

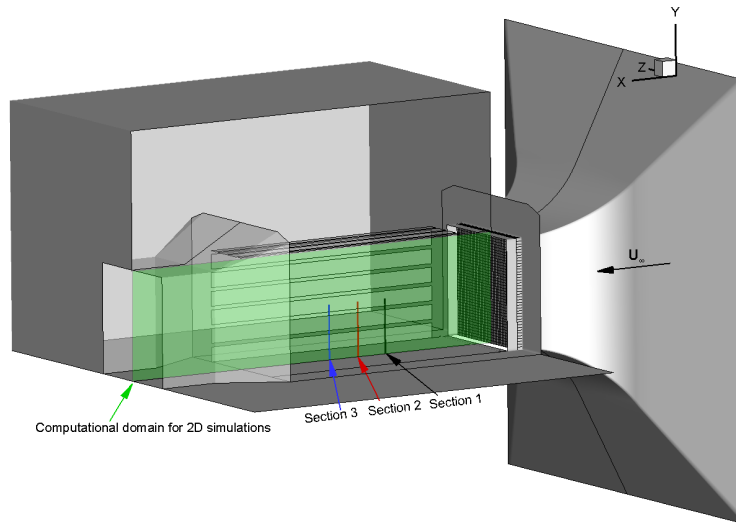


Fig. 2: View of the modeled reduced scale short wind tunnel (FP). Sections 1, 2 and 3 indicate the locations where the measurements were taken and compared with simulations (section 1, $x=0.57$ m; section 2, $x=0.74$ m; section 3, $x=0.92$ m).

hot wire anemometry to determine mean longitudinal velocity profiles (\bar{u}), turbulence intensity (I_u), turbulent length (L_u) and time scales (T_u), and power spectral density (PSD). All the experiments were performed at various freestream velocities ($U_\infty = 14, 17$ and 20 m/s). For brevity, only the results for $U_\infty = 20$ m/s are discussed, the cases of other velocities supporting the conclusions drawn from the 20 m/s case.

4.1 Validation study

To calibrate the model parameters, the turbulence model and to assess the influence of the grid, 3D simulations of the flow inside the empty reduced scale wind tunnel (FP) were carried out at various freestream velocities. The results are compared with hot wire measurements. For all simulations, uniform conditions were imposed at the inflow assuming constant velocity, and the initial turbulence intensity and turbulent length scale ($I_u=1\%$ and $L_u=0.012$ m) were specified. At the outflow, extrapolation conditions were imposed and pressure is forced to be equal to the atmospheric pressure. The geometry, being symmetric with respect to the vertical mid-longitudinal plane ($y=0$ mm), only half geometry is simulated and symmetric boundary conditions are imposed at the mid plane. At all surfaces, no slip boundary conditions are set, while no special treatment is imposed across the wall slots since the simulated experimental test chamber is confined by external solid walls to accurately reproduce the physical model of the FP.

The model geometry and the 2D computational domain is reported in figure 2. In the figure, sections 1, 2 and 3 indicate the locations where measurements are taken and compared with the numerical results obtained on a grid consisting of 2.6 M cells (for the full 3D model geometry case).

The distributions of the streamwise mean velocity normalized by the freestream value and of the turbulence intensity (I_u) at the three different measurement locations (section 1: $x=0.57$ m, section 2: $x=0.74$ m and section 3: $x=0.92$ m) is shown in Figure 3. The results show good agreement between experiments and numerical simulations. The differences in the near vicinity of the wall ($z/\delta < 0.07$) are likely due to wind tunnel surface floor defects that were not taken into account in the simulations and that affect the development of the boundary layer.

4.2 Boundary layer development in a short wind tunnel

In order to design the grid of horizontal bars (dimensions and spacing) and characterize their influence on the boundary layer development, two-dimensional numerical simulations were first carried out

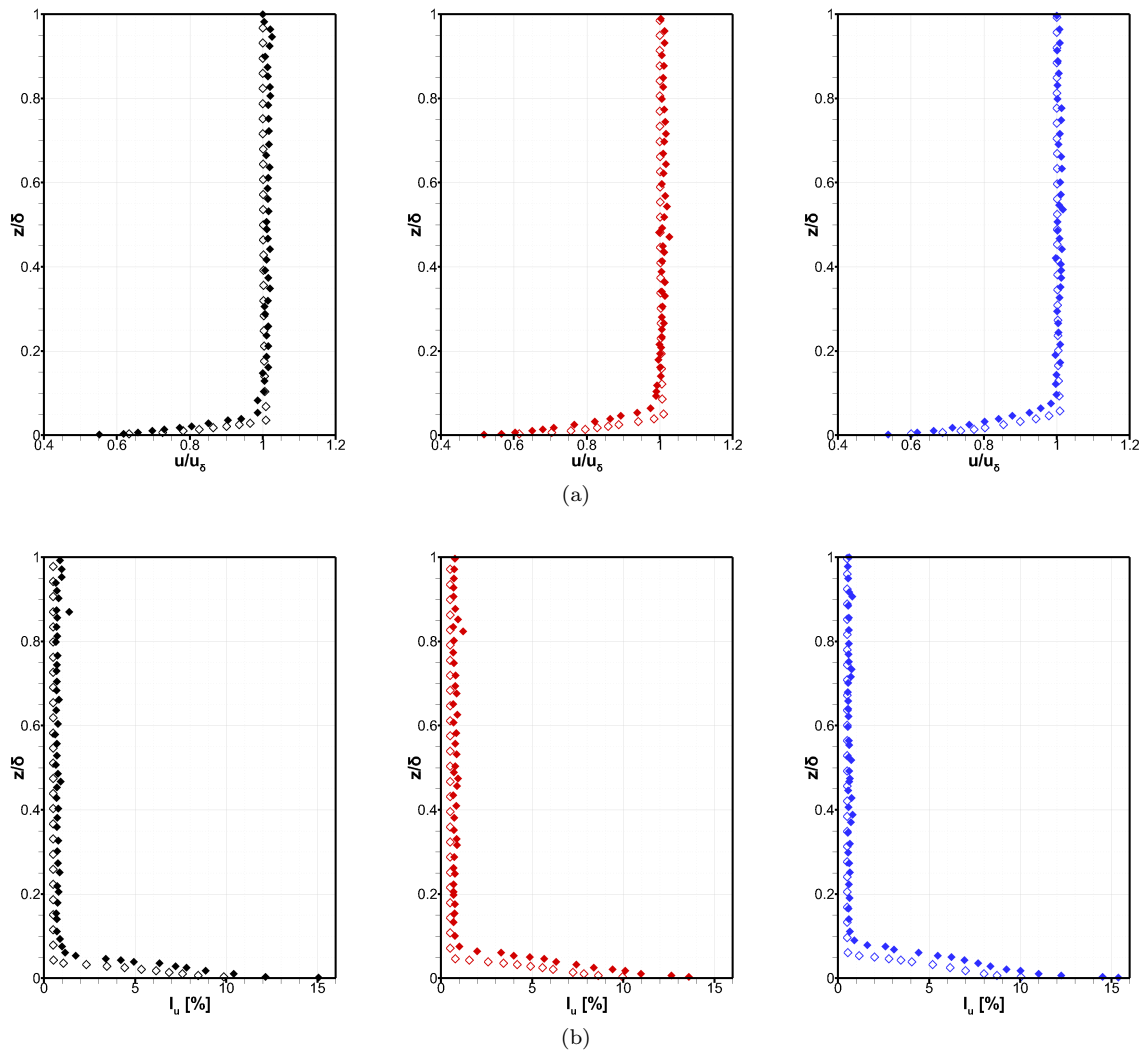


Fig. 3: Distributions of the streamwise mean velocity component (a) normalized by the velocity at the edge of the boundary layer and of the turbulent intensity (b) as a function of the normalized distance from the ground (z/δ) (\blacklozenge , experimental measurements; \diamond , numerical results). black symbols, section 1; red symbols, section 2; blue symbols, section 3.

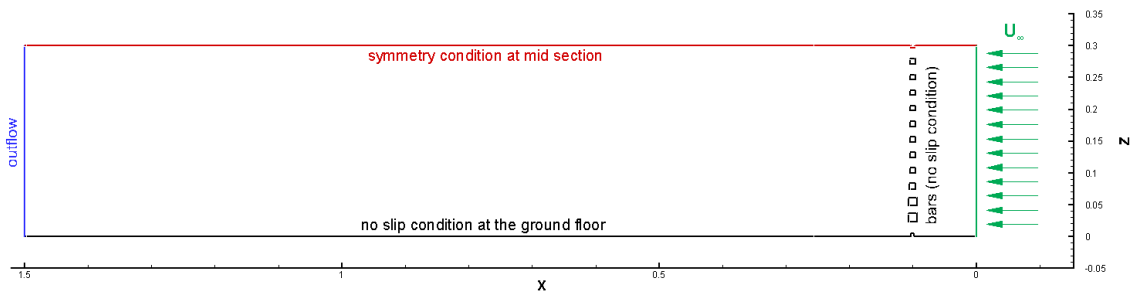


Fig. 4: Computational domain for the two-dimensional simulations.

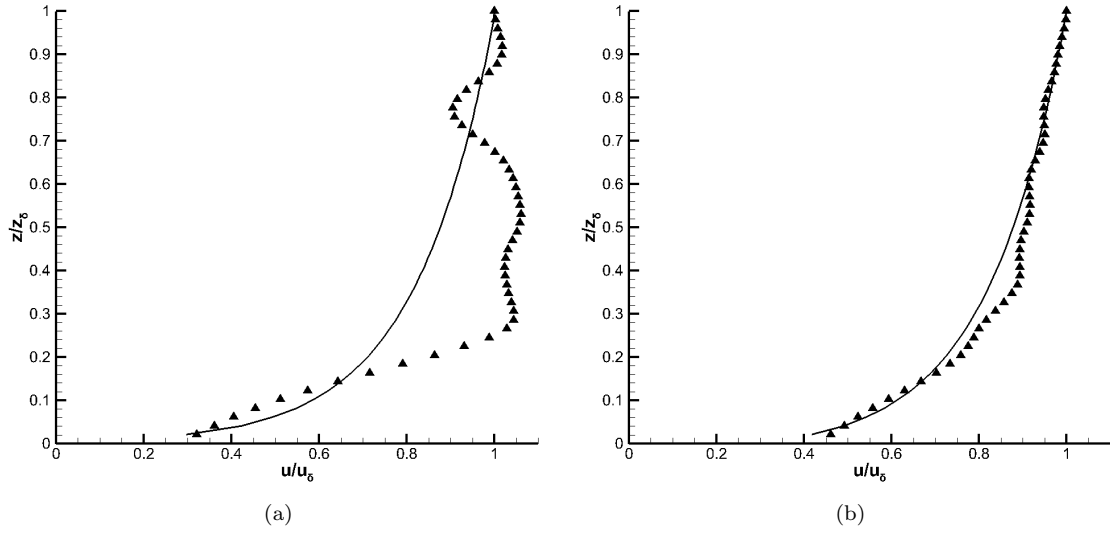


Fig. 5: The computed velocity profile (\blacktriangle) in outer variable (z/δ). (a) results for equally spaced squared section bars of equal dimensions; (b) results for squared section bars of different dimensions.

considering the longitudinal vertical mid-plane of the FP test chamber and imposing a wind velocity of 20 m/s (see figure 4).

The computational domain used for two-dimensional computations is outlined in figure 4. For all simulations, a structured mesh was assessed and a mesh sensitivity analysis was carried out by considering 4 different grids identified as M_1 , M_2 , M_3 and M_4 , whose total number of cells (N_T) is 20908, 83632, 334528, 1338112, respectively. The mesh sensitivity analysis was performed by surveying a quantity of interest (in our case the mean velocity profile). The criterion was that the quantity of interest does no longer change more than 1% while refining the mesh. At each successive refinement, the mesh spacing was halved in both directions.

Several simulations have been performed (only the results on the finest mesh M_4 are discussed), by varying the vertical spacing and the cross dimensions of the bars (we only consider bars of squared cross-section). The device consists of 25 bars initially assumed uniformly spaced in the vertical direction ($S=14\text{mm}$ measured as the distance between two consecutive bars and having the same dimension $D=10$). The dimensions and the spacing of the bars have been varied through a trial and error procedure imposing that the standard deviation (σ_V) of the computed mean velocity from the logarithmic law to be less than $O(10^{-2})$, with σ_V defined as

$$\sigma_V = \frac{1}{N_Z} \sqrt{\sum \left(\bar{u}(x, z_n) - \frac{u_\tau}{K} \ln \frac{z_n}{z_0} \right)^2} \quad (7)$$

N_Z being the total number of mesh points in the z direction at the given streamwise position x .

The profiles of the streamwise mean velocity component in outer variable z/δ are reported in figure 5; the analytical velocity distribution (equation 2) is also reported for comparison purposes. The results obtained on uniformly spaced bars (the distance between two consecutive bars is 14mm) of equal size (10mm) for which $\sigma_V = 1.4 \cdot 10^{-1}$ are shown in panel (a). In order to reduce such large deviation, the spacing and the dimensions of the bars were varied through a trial and error procedure imposing that the standard deviation of the mean velocity from the logarithmic law is halved, which is a good compromise between the constraint on the deviation from the log law and the mechanical, design and manufacturing ones (results are shown in panel (b)). The resulting geometrical parameters of the bars are reported in table 1, where all quantities are nondimensionalized with respect to the size of the first bar lying on the wall.

4.3 Boundary layer development in short wind tunnel equipped with a grid of horizontal bars

Based on the previous results, a grid of horizontal unequally spaced bars of unequal cross-section (the dimensions and spacings are given in table 1) was designed and manufactured. The grid was installed

Table 1: Geometrical parameters of optimized horizontal bars (d being the dimension of the first near wall bar; d=5 mm). B_1 is the bar on the wind tunnel floor and B_{13} is the bar located farthest from the wall.

Bar (B)	B_1	B_2	B_3	B_4	B_5	B_6	B_7	B_8	B_9	B_{10}	B_{11}	B_{12}	B_{13}
Dimension (D/d)	1	2.48	2.48	1.92	1.76	1.76	1.76	1.68	1.6	1.6	1.52	1.52	1.36
Spacing (S/d)	0	3.71	2.43	2.71	3.15	3.15	3.15	3.19	3.27	3.31	3.35	3.39	3.47

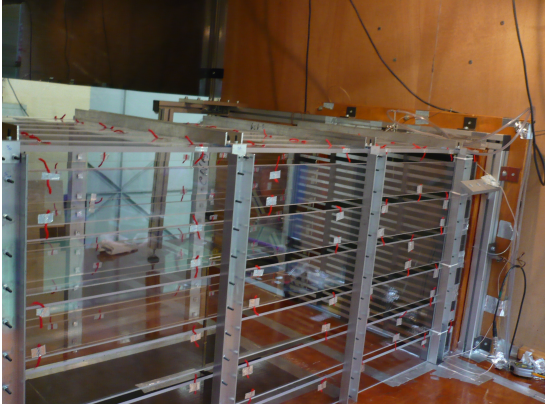


Fig. 6: View of the grid of horizontal bars inserted in the wind tunnel downstream of the convergent at the entrance of the test chamber.

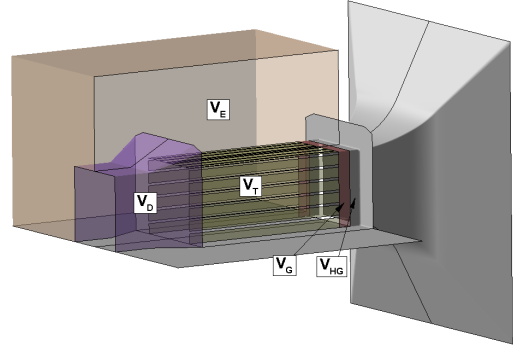


Fig. 7: View of the 3D numerical model of FP.

Table 2: Mesh sensitivity analysis: N_T is the total number of cells.

Block	N_T	Type of grid
V_D	199919	unstructured
V_T	1351296	structured
V_G	195594	structured
V_{HG}	139776	structured
V_E	545934	unstructured

downstream of the convergent at the entrance of the test chamber of the wind tunnel. Experimental measurements and numerical simulations have been carried out for various wind velocities. The experimental setup is shown in figure 6. For the simulations, the full reduced scale modified wind tunnel geometry (modified FP) has been discretized considering 5 blocks (see figure 7) corresponding to: the volume of the diffuser (V_D), the test chamber (V_T), the volume surrounding the grid of horizontal bars (V_G), the region between the honeycomb and the horizontal bars (V_{HG}), and one block for the volume between the original wind tunnel and the cage (V_E). The total number of cells per block is given in table 2.

Power law and ABL comparison

To compare the simulated ABL profile (the numerical and the experimental one) against full scale measurements, the scale factor (between the model ABL and the natural ABL) must be determined as suggested by Cook [5], namely

$$S = \frac{91.3(z-d)_M^{0.491}}{L_{uM}^{1.403} z_{0M}^{0.088}} \quad (8)$$

where the subscript M stands for the model values and L_u is computed from equation 4. Since the integral length scale varies with x , the scale factor varies accordingly. In particular, at $x_1=0.57\text{m}$: $S_1=12000$ for which the total depth of the simulated ABL is $\delta_1=3600\text{m}$; at $x_2=0.74\text{m}$: $S_2=6500$ and

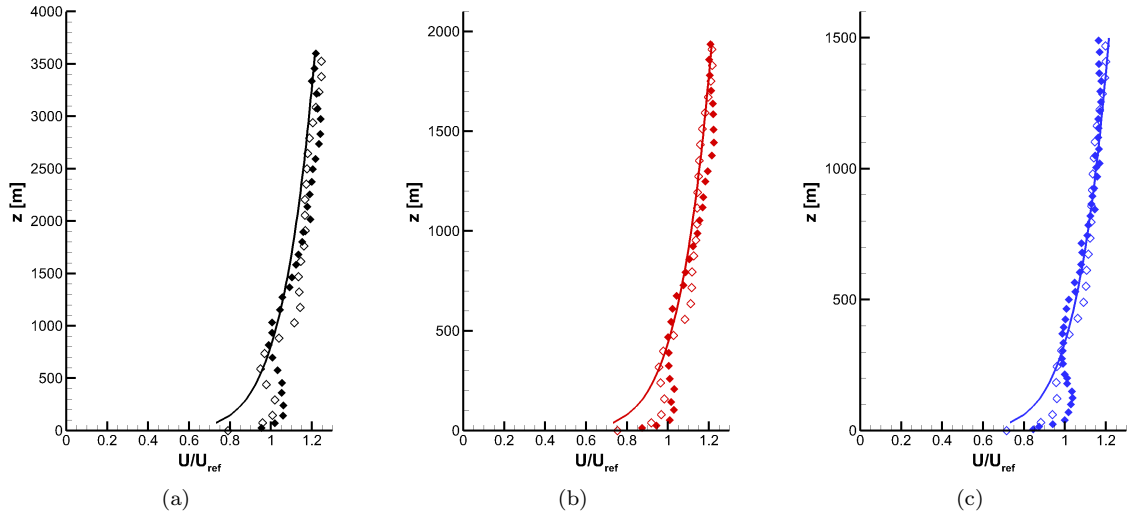


Fig. 8: Power law representation of the mean velocity profiles (\blacklozenge , experimental measurements; \diamond , numerical results; $-$, equation 2). a) section 1; b) section 2; c) section 3.

$\delta_2=1950\text{m}$; and at $x_3=0.92\text{m}$: $S_3=5000$ and $\delta_3=1500\text{m}$. In the majority of the ABL wind tunnel modeling, the scale factor ranges between 1:200 and 1:500. However, successful studies of ABL simulations are even for larger scales (1:2000 - 1:15000) ([18], [22]).

The comparison in the distribution of the longitudinal mean velocity component as a function of the distance from the ground is shown in real scale in figure 8 at the three sections. The experimental measurements, the numerical results and the power law (equation 2) are reported for comparison purposes. The power law exponent was obtained by adjusting the power law to best fit the experimental and numerical profiles and $\alpha=0.13$ was found, which indicates that the modeled ABL is representative of the flow over rough terrain, open sea or lakes with at least 5 km fetch and smooth flat country without obstacles [12]. Good collapse of the data is observed at all sections, with some differences in the near ground region ($z \sim 200\text{-}300\text{ m}$) or $z/\delta=0.2$ in scaled coordinates (i.e. near the wind tunnel floor). The ABL heights are scaled up from wind tunnel scale to full scale using Cook's scaling procedure [5] and the reference velocity is the velocity at a height of 22% of the atmospheric boundary layer depth.

The distributions of the measured and computed turbulence intensity (equation 3) at full scale are shown in figure 9. The figure confirms a rather good agreement between the numerical and experimental results at all sections, with the numerical results overpredicting the experimental values by approximately 1%. The figure also shows that numerical simulations and experiments underestimate (by 9% - 22%) the values obtained from the approximate relation $I_u = \frac{1}{\ln z/z_0}$ [13], for which the effects of background turbulence and the orography of the terrain have been neglected. However, the figure shows that the simulated and measured turbulence intensity exhibit the same qualitatively logarithmic dependency.

Integral length scales and power spectra

The distribution of the integral length scales L_u and L_v are reported at wind tunnel (figure 10a) and real (figure 10b) scales. As observed in previous studies of grid generated turbulence ([23]; [20]), the figure 10a shows an increase of the integral length scales in the downstream direction, and a collapse of L_u and L_v . In figure 10b the measured data is compared with the Eurocode and the ESDU ABL estimations ([13], [14]). The dashed line indicates the $\pm 20\%$ confidence level for the ESDU estimation. The figure shows that the data collapses reasonably well up to $z \sim 100\text{ m}$. At heights above 100 m L_u and L_v do not exhibit any significant variation as also observed in other studies [17], which is typical wind tunnel simulation methods [19].

The normalized power spectral densities of the longitudinal and normal velocity components were computed by a FFT using Welch's algorithm and zero-padding, and are reported in figure 11 at the different heights from the floor ((a), $z=32\text{ mm}$; (b), $z=92\text{ mm}$) and at the three sections

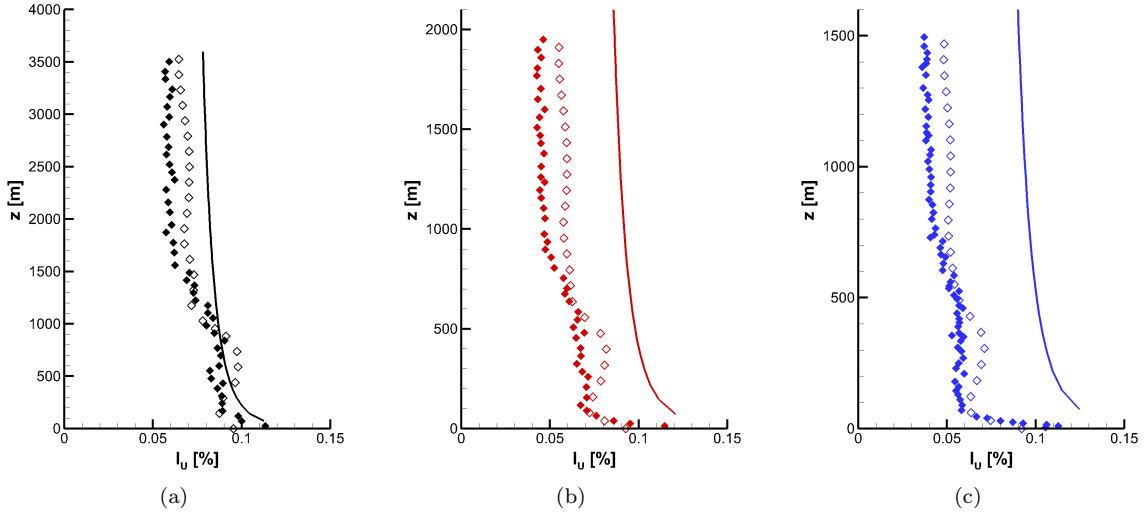


Fig. 9: Turbulence intensity distribution as a function of the distance from the ground (\blacklozenge , experimental measurements; \diamond , numerical results; $-$, Eurocode estimation). a) section 1; b) section 2; c) section 3.

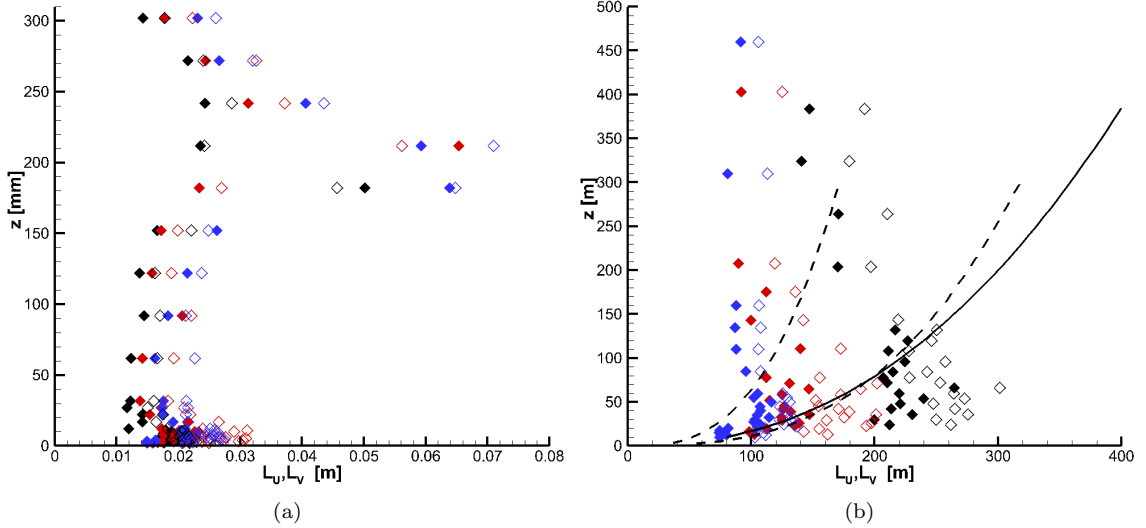


Fig. 10: Distribution of the integral length scale at wind tunnel (a) and full (b) scale for 20 m/s wind. full symbols, L_u ; hollow symbols, L_v (section 1, \blacklozenge ; section 2, \redlozenge ; section 3, \bluelozenge ; Eurocode, $-$; ESDU, $--$)

downstream of the grid (see figure 2). In the figure, the Von Karman spectra (equations 5 and 6) is also reported. The figures show a good collapse of the measured S_u (left panels) and S_v (right panels) at all sections. The spectra of the modeled ABL exhibits approximately a one-decade $-5/3$ decay, and compare well with the Von Karman relations throughout the measured frequency range. In the inertial high frequency (low energy content) range, they exhibit a roll up, which is to be ascribed to aliasing error and to anemometer response to electronic white noise ([25], [15]). The effect on the spectra related to confinement due to wind tunnel walls as reported in previous studies [24] was not observed here, such effect being suppressed by the slotted walls.

5 Conclusions

The present work focused on the modeling of the atmospheric boundary layer in a short wind tunnel. In order to use the wind tunnel for a variety of applications (automotive and train aerodynamics, wind effects on structures, etc.) the analysis is concentrated on devices that would allow a reversible

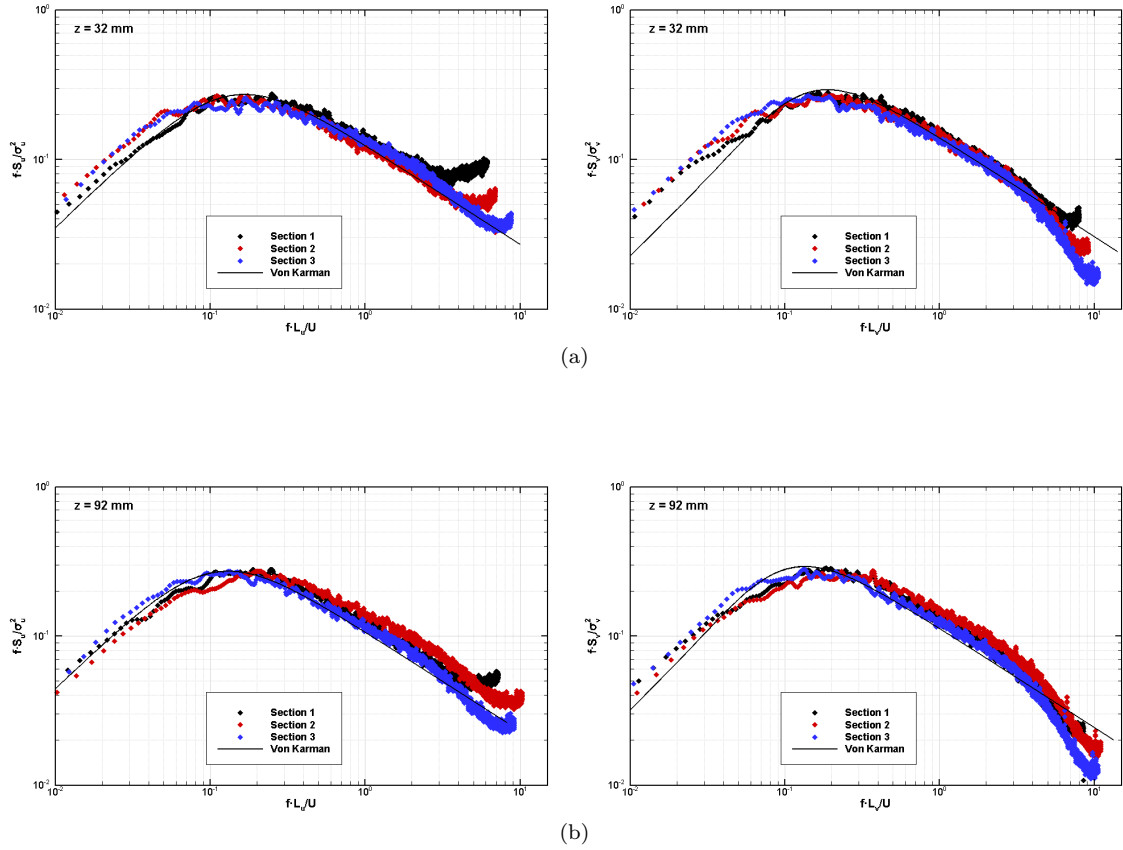


Fig. 11: Premultiplied normalized power spectral density (left panels, fS_u/σ_u^2 ; right panels, fS_v/σ_v^2) at $z=32$ mm and $z=92$ mm. \diamond , experimental measurements; $-$, Von Karman power spectrum.

configuration. The study relied on experimental and numerical investigations. The proposed methodology consists of a passive flow control device composed of a grid of bars of squared cross-section of different dimensions placed horizontally in the transverse direction. The Reynolds Averaged Navier Stokes equations were solved by second order finite volume method based on the SST $k-\omega$ model of [21], and the velocity and turbulence intensity were measured by hot-wire anemometry. The results were also compared with the semi-analytical predictions of the Eurocode. The mean velocity and the turbulence intensity profiles measured in the empty wind tunnel showed a good agreement between experiments and numerical simulations, and confirmed that the flow developing in a low turbulence intensity ($\sim 1\%$) short wind tunnel does not attain properties typical of an atmospheric boundary layer.

Inserting the grid of horizontal bars in the tunnel proved to be effective in reproducing the main characteristics of an atmospheric boundary layer in a short wind tunnel. The experimental measurements and the numerical simulations are in a good agreement at various sections downstream of the grid. The measured longitudinal velocity component was found to well approximate the power law distribution typical of an ABL when scaled as proposed by [5]. Similarly, the estimated integral length scales were found to fall in the 20% confidence level of the ESDU. The measured power spectral densities of the longitudinal and normal velocity components were also found to obey the Von Karman laws across the measured frequency range. However, the turbulence intensity was generally underestimated, which lead us to conclude that further investigations should be performed combining the passive system here discussed with roughness elements, which are known to increase wind turbulence [19].

For the design of the grid, several elements were considered. The shape of the bars was chosen to be squared to limit the variability of the turbulent field. In order to have a better control on the simulated ABL, a symmetric grid with respect to the horizontal longitudinal mid plane was chosen, and the lowest (and the highest) bar was attached to the wind tunnel floor (ceiling). Considering a split of the lower half of the grid into tiers, the porosity of the grid (calculated with $\beta = (1 - \frac{D}{S})^2$) is

smaller in the first tier with respect to the second one which is smaller than the third tier (0.1; 0.18; 0.27). The ratio of the sum of the bars from tier 1 and the sum of the bars in tier 2 is equal to the ratio of the sum of the bars from tier 2 and the sum of the bars from tier 3.

Acknowledgements

This work was carried out at the Institut Aérotechnique (IAT) that provided full access to wind tunnel facilities and equipments. The valuable input of professor Francesco Grasso and the technical assistance of Bruno Bassery (IAT staff) is acknowledged

Funding sources

This research did not receive any specific grant from funding agencies in the public, commercial, or not-for-profit sectors.

References

1. Alan G. Davenport, Wind tunnel testing: a general outline, The Boundary Layer Wind Tunnel Laboratory, The University of Western Ontario, Faculty of Engineering Science London, Ontario, Canada, N6A 5B9, (2007).
2. ANSYS, Ansys Fluent, 14.0 Theory Guide, ANSYS Inc, 390, (2011).
3. Balendra, T and Shah, DA and Tey, KL and Kong, SK, Evaluation of flow characteristics in the NUS-HDB Wind Tunnel. *Journal of Wind Engineering and Industrial Aerodynamics*, 90 (6), 675–688, (2002).
4. Barbosa, PHA and Cataldi, M and Freire, APS, Wind tunnel simulation of atmospheric boundary layer flows, *Journal of the Brazilian Society of Mechanical Sciences*, 24, 177–185, (2002).
5. Cook, NJ, Determination of the model scale factor in wind-tunnel simulations of the adiabatic atmospheric boundary layer, *Journal of Wind Engineering and Industrial Aerodynamics*, 2 (4), 311–321, (1978).
6. Counihan, J, A method of simulating a neutral atmospheric boundary layer in a wind tunnel, *AGARD Conference Proceedings*, 43, (1969).
7. Counihan, J, An improved method of simulating an atmospheric boundary layer in a wind tunnel, *Atmospheric Environment*, 3 (2), 197–214, (1969).
8. Counihan, J, Simulation of an adiabatic urban boundary layer in a wind tunnel, *Atmospheric Environment*, 7 (7), 673–689, (1973).
9. Counihan, J, Adiabatic atmospheric boundary layers: a review and analysis of data from the period 1880–1972, *Atmospheric Environment*, 9 (10), 871–905, (1975).
10. De Bortoli, ME and Natalini, B and Paluch, MJ and Natalini, MB, Part-depth wind tunnel simulations of the atmospheric boundary layer, *Journal of Wind Engineering and Industrial Aerodynamics*, 90 (4-5), 281–291, (2002).
11. Diana, G and De Ponte, S and Falco, M and Zasso, A, A new large wind tunnel for civil-environmental and aeronautical applications, *Journal of Wind Engineering and Industrial Aerodynamics*, 74, 553–565, (1998).
12. Dyrbye, Claës and Hansen, Svend Ole, Wind loads on structures, John Wiley and Sons LTD, (1997).
13. European Standard, Eurocode 1: Actions on structures, European Comitee for Standardization, (2005).
14. Sheets, ESDU Data, Characteristics of atmospheric turbulence near the ground, Part II, Single point data for strong winds (neutral atmosphere), *Engineering Sciences Data Item 85020*, (1990).
15. Freymuth, Peter and Fingerson, Leroy M, Hot-wire anemometry at very high frequencies: effect of electronic noise, *Measurement Science and Technology* 8 (2), 115, (1997).
16. Hasegan L. V., Degeratu M., Sandu L., Georgescu A. M., Cosoiu C. I., *Modelare experimentală și numerică în ingineria vântului*, Printech, (2008).
17. Hohman, TC and Van Buren, T and Martinelli, L and Smits, AJ, Generating an artificially thickened boundary layer to simulate the neutral atmospheric boundary layer, *Journal of Wind Engineering and Industrial Aerodynamics*, 145, 1–16, (2015).
18. Hunt, JCR and Fernholz, H, Wind-tunnel simulation of the atmospheric boundary layer: a report on Euromech 50, *Journal of Fluid Mechanics* 70 (3), 543–559, (1975).
19. Kozmar, Hrvoje, Characteristics of natural wind simulations in the TUM boundary layer wind tunnel, *Theoretical and applied climatology*, 106 (1-2), 95–104, (2011).
20. Liu, Rui and Ting, David S-K and Checkel, M David, Constant Reynolds number turbulence downstream of an orificed perforated plate, *Experimental thermal and fluid science*, 31 (8), 897–908, (2007).
21. Menter, Florian R, Two-equation eddy-viscosity turbulence models for engineering applications, *AIAA journal*, 32 (8), 1598–1605, (1994).
22. Meroney, Robert N, Wind-tunnel simulation of the flow over hills and complex terrain, *Journal of Wind Engineering and Industrial Aerodynamics*, 5 (3-4), 297–321, (1980).
23. Moradian, Niloofar and Ting, David S-K and Cheng, Shaohong, The effects of freestream turbulence on the drag coefficient of a sphere, *Experimental thermal and fluid science*, 33 (3), 460–471, (2009).
24. Peterka, JA and Hosoya, N and Dodge, S and Cochran, L and Cermak, JE, Area-average peak pressures in a gable roof vortex region, *Journal of Wind Engineering and Industrial Aerodynamics*, 77, 205–215, 1998.
25. Saddoughi, Seyed G and Veeravalli, Srinivas V, Hot-wire anemometry behaviour at very high frequencies, *Measurement Science and Technology*, 7 (10), 1297, (1996).

-
26. Stathopoulos, Ted and Baniotopoulos, Charalambos C, Wind effects on buildings and design of wind-sensitive structures, SpringerWienNewYork, (2007).
 27. Tieleman, Henry W, Wind tunnel simulation of wind loading on low-rise structures: a review, Journal of wind engineering and industrial aerodynamics, 91 (12-15), 397-408, (2008).